

¹ Department of Atmospheric Sciences, National Central University, Jhong-Li, Taiwan

² Department of Marine, Earth and Atmospheric Sciences, North Carolina State University, Raleigh, NC, USA

The influence of mesoscale mountains on vortex tracks: shallow-water modeling study

C.-Y. Huang¹, Y.-L. Lin²

With 10 Figures

Received 1 November 2005; Accepted 29 January 2007

Published online 18 February 2008 © Springer-Verlag 2008

Summary

This study utilizes a shallow-water numerical model to investigate the influences of mountain topography on an approaching vortex on an f -plane. Systematic numerical experiments show that vortex track deflection is significantly dependent upon several parameters, namely the maximum tangential flow speed of the vortex (V_{\max}), the basic flow (U), the fluid depth (H), the radius of V_{\max} (R), the mountain height (h), and L_m which, in the presence of mean flow, is represented by L_y defined as the mountain half-width in the direction normal to the vortex movement. Accordingly, there exist several nondimensional parameters, the vortex Froude number, V_{\max}/\sqrt{gH} , the basic-flow Froude number, U/\sqrt{gH} , the nondimensional mountain height, h/H , and the nondimensional vortex size R/L_m . The northward track deflection for a westbound vortex is significantly reduced by increased U/\sqrt{gH} . However, the direction of track deflection is primarily controlled by R/L_m , with respect to the nondimensional height, h/H . Leftward (facing downstream) deflection can be expected with $HL_m/hR > 0.5$ or more strictly $L_m/R > 0.3$, for typical conditions, $h/H < 0.8$.

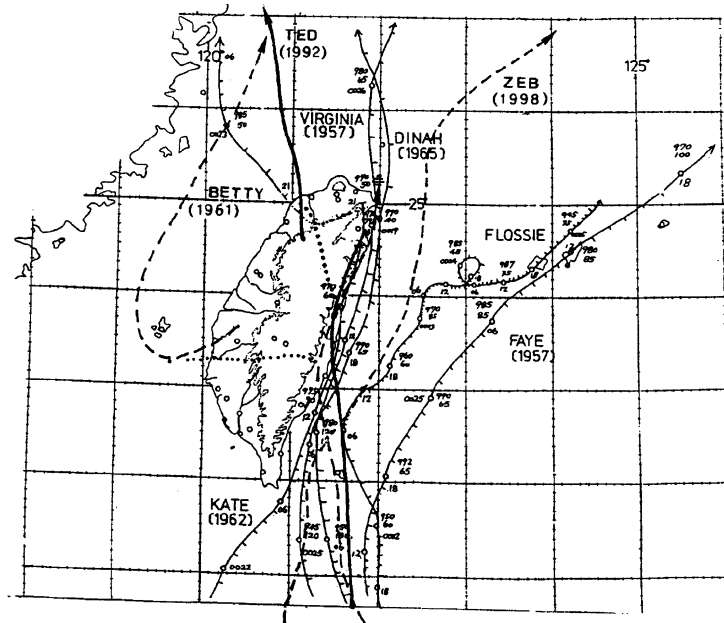
With the exclusion of explicit horizontal momentum diffusion, the vorticity budgets are essentially balanced by vorticity advection and vorticity stretching (associated with divergence) with the vorticity advection (stretching) being responsible for upstream rightward (leftward) deflection. A vortex tends to move in a clockwise path around a wider and

lower mountain. With a sufficiently large h/H (high mountain), the track of a vortex becomes rightward (counterclockwise) as a result of the more dominant vorticity advection. There is a transition of track deflection of a vortex from leftward to rightward for a decreasing mountain aspect ratio of L_y/L_x (where L_x is the mountain half width in the direction parallel to the vortex movement) which indicates that leftward (rightward) track deflection will be more dominant for a westbound (northbound) vortex past meridionally elongated mountains, such as the Central Mountain Range (CMR) of Taiwan.

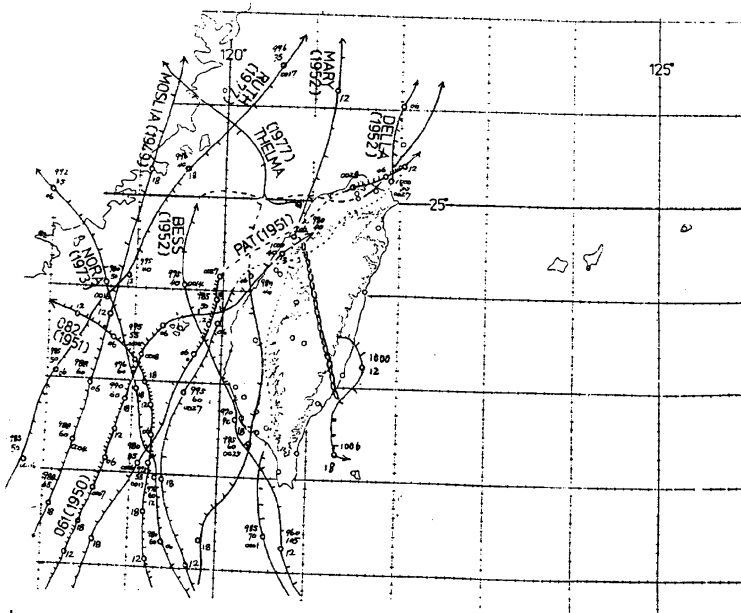
1. Introduction

The vortex drift past a mountain is a very intriguing phenomenon, in particular, with the track deflection to be anticipated for various mountains. In reality, Taiwan is an isolated mesoscale island where the Central Mountain Range (CMR) rises to about 4 km in height and stretches approximately 300 km from north-northeast to south-southwest and 100 km wide. Such a mountainous island provides an ideal setting for the study of the vortex track deflection. According to an extensive observational study of more than 100 typhoons, Wang (1980) pointed out that typhoons encountering Taiwan exhibit significant variation in the direction and continuity of their tracks. Similar variation with the tracks has also been observed with tropical cyclones (TCs) near other

Correspondence: Ching-Yuang Huang, Department of Atmospheric Sciences, National Central University, Jhong-Li, Taiwan 32001, Taiwan (E-mail: hcy@atm.ncu.edu.tw)



a



b

Fig. 1. Tracks of northbound typhoons moving (a) to the east and (b) to the west of Taiwan (Courtesy of Wang 1980)

mountainous areas, such as the mountains of Hispaniola in the Caribbean, the mountains of Luzon in the Philippines, and the Sierra Madre mountains of Mexico.

Most typhoons (about three-fourth of the total cases) in the past approached Taiwan from the east, the southeast, or the south. Fewer northbound typhoons have approached Taiwan than have westbound typhoons. Figure 1 shows the tracks of some northbound typhoons passing over or around Taiwan. Northbound typhoons can be deflected leftward or rightward by the CMR, sim-

ilar to the westbound typhoons; however, rightward deflection appears to occur more frequently than leftward deflection (Fig. 1).

In light of the complexities associated with track deflection of a typhoon past the CMR, numerical studies became the primary approach in the past. Most of these studies, however, were focused on simulations of westbound typhoons using different primitive-equation models (e.g., Chang 1982; Bender et al. 1987; Yeh and Elsberry 1993a, b; Huang and Lin 1997; Lin et al. 1999, 2002, 2005; Lin 2007). Chang (1982) found a

cyclonic curvature of the track of an idealized westbound typhoon (i.e., northward deflection upstream of the mountain) and speculated that its northward deflection is related to the effects of latent heating to the right of the vortex center. The northward deflection of idealized westbound typhoons was also demonstrated in the modeling study by Yeh and Elsberry (1993a, b) for an elliptic mountain somewhat larger than the CMR. Some forecast model results (e.g., Bender et al. 1987) also exhibited northward deflection in the tracks of stronger and faster realistic typhoons on a β -plane environment. Other modeling studies for weaker and smaller idealized vortices have shown leftward or southward deflection in the tracks of westbound vortices (e.g., Huang and Lin 1997; Lin et al. 1999). The above studies of real and idealized typhoons contained a variety of factors affecting the typhoon track, such as impinging angle of the vortex, varying environmental flow and stratification, diabatic heating, surface friction, boundary-layer mixing, or β -effects, rendering an explanation for track deflection far less than certain.

In a stratified fluid, southward deflections have been numerically simulated with westbound drifting vortices approaching an idealized CMR (Huang and Lin 1997; Lin et al. 1999, 2005; Lin 2007). Based on the systematic experiments using a primitive-equation (PE) model without surface friction and PBL effects, Lin et al. (2005) found that track deflection is mainly dominated by three nondimensional controlling parameters, i.e., V_{\max}/Nh (the vortex Froude number), U/Nh (the basic-flow Froude number) and R/L_y (the nondimensional vortex size), which are among eight possible dimensional parameters including U (the basic flow speed), V_{\max} (maximum tangential wind of the initial vortex), N (environmental stability frequency), f (the Coriolis parameter), L_x (the mountain length scale in the direction of the vortex movement), L_y (the mountain length scale in the direction normal to the vortex movement), R (the radius of V_{\max}), and h (the mountain height). Surprisingly, the basic-flow Froude number was found to play no major role in the direction of track deflection, though it does influence significantly the degree of deflection. Due to the nature of a mesoscale vortex at a relatively shorter time scale as passing mesoscale mountains similar to Taiwan topography,

the Rossby number (U/fL) that measures the rotation effects does not play a significant role in the track deflection. The vortex track tends to be discontinuous (continuous) and deflected southward for smaller (larger) V_{\max}/Nh and R/L_y with stronger (weaker) orographic blocking. A discontinuous track is associated with a developing lee vortex that takes over the upstream parent vortex at lower levels in the stratified fluid.

In this study, we intended to investigate the problem in a simpler environment by adopting a shallow water (SW) model. SW models have also been employed to study vortex track deflection problems in earlier studies. Results from one SW model show that leftward deflection was present with a vortex drifting toward the CMR from the southeast (Smith and Smith 1995). In our study, we are interested in studying the track deflection for a vortex from south or east in a simple environment, using idealized terrain representative of the CMR. Kuo et al. (2001) showed that a vortex in a SW model tends to move clockwise around an elliptic mountain on both f and β -planes in a quiescent fluid, and that the clockwise motion is relatively insensitive to vortex intensity. For anticyclonic curvature of a cyclone track to occur, L_y has to be comparable to or larger than the vortex size, or more specifically R . This is consistent with the leftward deflection for a vortex approaching the Sierra Madre Mountains of Mexico simulated by a SW model (Zehnder 1993; Zehnder and Reeder 1997). The characteristic length scale of the Sierra Madre Mountains is comparable to that of the cyclone. These SW studies have provided some insights into track deflection or looping problem for larger or synoptic-scale mountains, however, they have not been applied to mesoscale mountains on an f -plane. In this study, in order to simplify the dynamics, we will not consider the beta effects (e.g., Chan and Williams 1987; Smith 1993). Instead, we will focus on the track deflection of a vortex past idealized CMR on an f -plane. We aim at exploring some controlling parameters for such a vortex track deflection by taking a SW model (SWM) approach and intend to propose track deflection mechanisms by studying the vorticity budgets. Upstream track deflection in the presence of basic flow for Taiwan's CMR will also be investigated in this study, which was not addressed by the above-mentioned studies. We

plan to clarify the problems associated with the track deflection by examining the relevant control parameters in the shallow-water system. This SWM study will be followed by a companion paper using a mesoscale cloud model. The dominant nondimensional parameters found from this SWM study will provide more understanding of the basic dynamics and provide a guidance for the primitive equation (PE) modeling studies for realistic typhoons past a mesoscale mountain.

In Sect. 2, the SW model will be introduced. In Sect. 3, we will make scale analysis to identify some potential nondimensional controlling parameters for track deflection of a vortex impinging on a mesoscale mountain. In Sect. 4, the characteristic features of the simulated tracks are presented with parameter sensitivity study. Vorticity budget analyses will be performed in Sect. 4 to identify possible mechanisms of track deflection. Based on the argument on control parameters in Sect. 3 and the mechanisms discussed in Sect. 4, we provide a quantitative analysis of the hypothesized nondimensional parameters for track deflection in Sect. 5. In addition, to make the study more complete, we perform some sensitivity tests on vortex profiles, reduced gravity, and the Coriolis parameter, which have not been highlighted by earlier studies. Finally, concluding remarks will be given in Sect. 6.

2. The model description and experimental designs

2.1 The numerical model

The numerical experiments in this study use a SW model whose governing equations and numerics are described in the Appendix. A finite-difference SW model is used to study the movement of a vortex drifting over a bottom topography in a one-layer homogeneous fluid. Thus, our simulation is only descriptive of a long-wave approximation to hydrostatic motions and does not include the nonhydrostatic dispersive behaviors of shallow water (e.g., Nadiga et al. 1996; Wedi and Smolarkiewicz 2003). The fluid depth is set to 5 km with an imposed gravitational acceleration of 9.8 m s^{-2} , following similar earlier SW modeling studies (e.g., Smith et al. 1997; Kuo et al. 2001). Note that this is an effective depth, which produces realistic responses to an imposed

vortex, similar to those occurring in the real atmosphere. We will demonstrate that, with these settings, our SW model is able to reproduce many flow features which are commonly simulated by other SW and PE models. Since no boundary layer processes and surface friction are included in the SW model, the simulated vortex will behave like a drifting cyclone provided that numerical dissipation has only minimal effects on the solution. Smith and Smith (1995) showed that effects of numerical dissipation, however, were inevitably present in their SW model over a long simulation time. The effects of numerical dissipation, which are essentially necessary for smoothing the shortest waves, would make an analysis of orographic effects on track deflection difficult, particularly for initially weaker and smaller vortices at longer departure distances. However, this uncertainty can be greatly reduced by using shorter, yet reasonable departure distances in additional sensitivity tests, within which the drifting vortex can be preserved before approaching the topography.

2.2 Vortex initialization

The height perturbations are partitioned into two components, resulting from the basic-flow in geostrophic balance and the vortex circulation in gradient-wind balance, respectively. The initial vortex is assumed to be nondivergent and purely rotational. An elliptic Poisson equation, based on nondivergence of the flow, is solved for height perturbations. A quasi-steady state of the basic flow past the terrain can be reached after a proper simulation time; a specific vortex then is injected into the steady flow after the simulation time (two days in this study).

The radial profile of tangential flow for the vortex, following Chang (1982), is prescribed as

$$V_{\theta} = V_{\max}(r/R) \exp\left\{\frac{1}{b}[1 - (r/R)^b]\right\}, \quad (1)$$

where b is a parameter controlling the tangential wind profile of the vortex. The combination of b and R actually determines the vortex size; a larger value of b gives a narrower vortex core with stronger radial gradients. Normally, the value of b ranges from 0.4 to 2 (e.g., Smith et al. 1997). Following Lin et al. (2005), $b = 2$ is chosen for most cases in this study. DeMaria (1985) showed that the vortex track is more sensitive to variation

of radial profiles in the outer regions of a vortex than in the inner vortex core. The dependence of topographically-induced track deflection on b has not been explored and will be examined in this study.

2.3 The numerical experiments

Model simulations are performed for vortices on the f -plane. The horizontal grid resolution is 20 km in both the x - and y -directions. A Gaussian mountain is prescribed with a peak height of 4 km at the domain center. The vortex center is initially positioned 1400 km from the mountain center. All prognostic variables are assumed to possess zero gradients at the lateral boundaries. In consideration of the computational efficiency, a split cubic advection scheme was employed in the simulations (see Appendix). The inherent dissipation of the advection scheme is still not sufficient to modulate the developing shorter waves as the vortex passes over a steep mountain. Hence, we also include a nonlinear horizontal mixing term in the prognostic equation of surface height perturbation. Linear horizontal diffusion terms with similar effects have been used by Smith and Smith (1995).

3. Scale analysis for track deflection

Before presenting the results of numerical experiments, scale analysis will be performed to identify potential parameters controlling vortex track deflection. Previous studies based on PE models have shed light on some parameter candidates (e.g., Lin et al. 2005). In the pseudo-inviscid SW system, the dynamics are relatively simple, with vorticity stretching and vorticity advection being the primary mechanisms affecting track deflection. Shapiro and Ooyama (1991) investigated the effect of divergence on a barotropic vortex without topography. Zehnder (1993) performed a scale analysis for a vortex past bottom topography on a β -plane. Similar to Zehnder (1993), the vorticity equation on an f -plane is given as

$$\frac{\partial \zeta}{\partial t} = -\mathbf{V} \cdot \nabla \zeta - (\zeta + f) \left(\frac{\partial u}{\partial x} + \frac{\partial v}{\partial y} \right). \quad (2)$$

The vortex stretching (divergence) term, i.e., the last term on the right-hand side of Eq. (2), is related to the thickness of the fluid layer (H) via the

continuity equation,

$$\frac{dH}{dt} + H \left(\frac{\partial u}{\partial x} + \frac{\partial v}{\partial y} \right) = 0, \quad (3)$$

where

$$H = H_0 + h' - h_B, \quad (4)$$

which is identical to Eq. (A.4). Thus, the divergence term may be expressed in terms of the thickness of the fluid layer as

$$\begin{aligned} -(\zeta + f) \left(\frac{\partial u}{\partial x} + \frac{\partial v}{\partial y} \right) &= \frac{(\zeta + f)}{H} \frac{dH}{dt} \\ &= \frac{(\zeta + f)}{H} \left[\frac{dh'}{dt} - \mathbf{V} \cdot \nabla h_B \right]. \end{aligned} \quad (5)$$

The gradient-wind balance (Shapiro and Ooyama 1991) is used to estimate the total change of the perturbation height far upstream of the topography,

$$\frac{dh'}{dt} \sim \frac{R}{gT} \left(\frac{V_{\max}^2}{R} + f V_{\max} \right), \quad (6)$$

where $T \sim R/V_{\max}$ is the Lagrangian time scale of the rotational flow. The Coriolis force is assumed to play a less significant role in the upstream track deflection as the vortex core approaches mesoscale topography, given the relatively short passage time. The second term inside the square bracket of the right-hand side of Eq. (5) has a scale as

$$\mathbf{V} \cdot \nabla h_B = (U + V_{\max}) \frac{h}{L_m} \approx V_{\max} \frac{h}{L_m}. \quad (7)$$

The substitution of V_{\max} for \mathbf{V} in Eq. (7) would indicate that an intense vortex core is more important than the basic flow for the resulting divergence near the topography. However, the vorticity advection in Eq. (2) for a vortex upstream of the topography is estimated as

$$\mathbf{V} \cdot \nabla \zeta \sim U \frac{\zeta}{R}, \quad (8)$$

which measures the upstream vortex advection simply by the basic flow.

If the effect of the orographically-induced depth change can be assumed to be more dominant than the variation of Lagrangian dynamic depth, it would require from Eqs. (5), (6), and (7) that

$$\frac{hR}{HL_m} > \frac{V_{\max}^2}{gH} = F_{\text{vor}}^2, \quad (9)$$

requiring a high mountain (h), a small mountain length (L_m), a large vortex (R), or a weak intensity (V_{\max}). A more precise analysis of Eq. (9) would require the use of local Froude number, which is actually dependent on local fluid depth and velocity. For a typical SW vortex, the value of the left-hand side of Eq. (9) will normally be greater than that of the right-hand side, and so the vortex Froude number F_{vor} may not be a good indicator for track deflection.

Local vorticity generation is controlled by vorticity advection and vorticity stretching. When vorticity stretching is more dominant than upstream vorticity advection, as a result of bottom topography effects, we must have from Eqs. (2), (5), (6), and (8):

$$\frac{hR}{HL_m} > \frac{U}{V_{\max}}, \quad (10)$$

which requires a steep mountain or a large vortex with high tangential velocity. Since the vorticity advection is estimated by Eqs. (8), (10) is more applicable when the vortex is located farther upstream. When the vortex is located near the mountain, the total vorticity advection in the vicinity of the mountain cannot be estimated simply by Eq. (8). Hence, the above analyses are only used to identify the set of control parameters, and provide a physical basis for the parameter regimes investigated in this study.

4. General track deflection of a vortex past mesoscale mountains

Before presenting our results for vortex track deflection, we would like to discuss the effect of the diffusion terms on the simulation. We conducted sensitivity experiments for a vortex past a mesoscale mountain (i.e., case TWB, see Table 2). The initial vortex has a V_{\max} of 40 m s^{-1} at $R = 150 \text{ km}$, with the center located 800 km east of the mountain peak. Figure 2 shows the simulated absolute vorticity and the associated flow velocity at 70 h using different options of horizontal diffusion when the vortex center is near the mountain. When the nonlinear second-order diffusion term (see Pielke 1984) is included in both the height and momentum equations, the intensity of the simulated vortex decreases considerably before it approaches the mountain (Fig. 2a). The damping induced by the second-order diffusion is

significantly reduced when the nonlinear diffusion term is included only in the height equation (Fig. 2b). On the other hand, when the fourth-order diffusion terms are applied with a very small nondimensional diffusion coefficient of 10^{-4} , defined as $K_H \Delta t / (\Delta x)^4$, in both height and momentum equations, the vortex intensity (Fig. 2c) remains as strong as in Fig. 2b. A slightly stronger vortex (Fig. 2d) can be preserved when the split cubic advection scheme is replaced with the unsplit bi-quintic advection scheme, but the position of the vortex center remains unchanged. Using a different horizontal diffusion form or a less-diffusive advection scheme does not change the southward track deflection for this case. Hence, we will use the nonlinear diffusion term to represent turbulent mixing in the following experiments. Without explicit horizontal momentum diffusion, vorticity budgets are determined by both the advection term and divergence term.

We first conduct a series of experiments for mountains larger than the CMR, as listed in Table 1. The center of the evolving vortex is tracked within a zone, of $100 \text{ km} \times 100 \text{ km}$, encompassing the center at the previous time step. The center can be defined by the vorticity or the flow speed in the searching zone, namely the vorticity center where the maximum vorticity exists, and the circulation center where the minimum flow speed exists. The maximum distance of upstream track deflection is defined as the maximum latitudinal distance of the vortex center from its initial latitude east of the centerline of the mountain.

Results indicate that all vortices in experiment groups A, B, C, and D of Table 1 are deflected southward near the mountains. It is also observed that a larger and weaker cyclone (e.g., case AD) experiences a relatively greater latitudinal deflection. The presence of an east-west oriented mountain range (i.e., experiment group C) generally reduces the southward deflection found with group A, due to the smaller length scale of L_y . The increase of basic flow speed in group B also results in less deflection of the vortex tracks; however, the reduction is not linear with respect to R or V_{\max} .

With mountain scales tripled in value to $L_x = 300 \text{ km}$ and $L_y = 600 \text{ km}$ for group D, the southward track deflection is not affected by V_{\max} or R (Table 1). At a moderate basic flow speed of 4 m s^{-1} , all vortices in group D are trapped by the mountain, with the parent vortex revolving

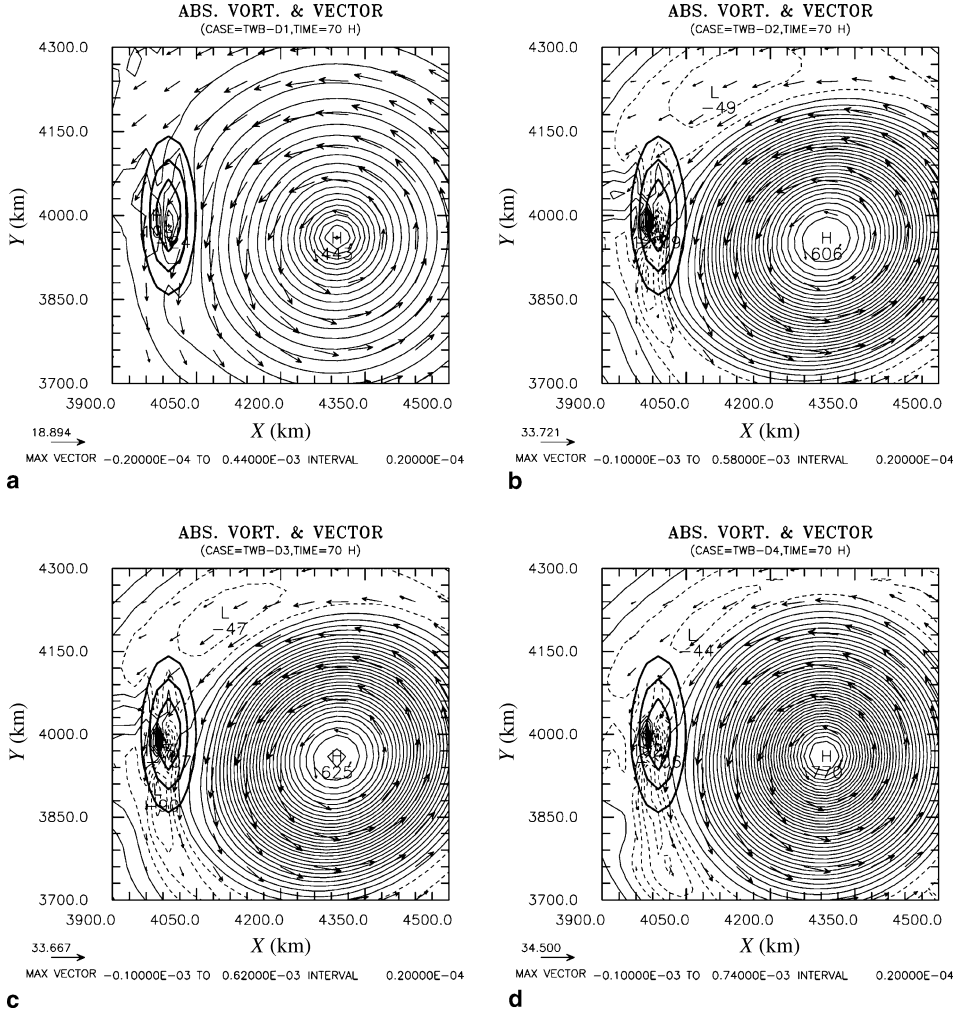


Fig. 2. The absolute vorticity and flow velocity vector for TWB at $t = 70$ h (a) using constant coefficient $c_H = 1$ in the nonlinear second-order diffusion terms for both height and momentum equations, (b) as in (a) but using $c_H = 2$ for the height equation only, (c) using the fourth-order diffusion with a nondimensional coefficient of 10^{-4} for both height and momentum equations and (d) as in (c) but using the unsplit bi-quintic advection scheme. The contour interval in each panel is $0.2 \times 10^{-4} \text{ s}^{-1}$. The solid (dashed) lines indicate positive (negative) contours and the wind has units of m s^{-1} in this figure and hereafter. The bold lines indicate the contours of 1-km, 2-km and 3-km mountain heights, respectively

around the mountain slope following an upstream southward deflection but the other vortex remains shedding downstream due to the advection by basic flow. Vortex trapping does not occur in the cases featuring a considerably smaller mountain, except with very weak basic flow. Vortex trapping also does not occur in group D when the basic flow speed is doubled to 8 m s^{-1} , and again not sensitive to V_{\max} and R .

Leftward (southward) track deflection was also simulated by Zehnder and Reeder (1997) for a vortex approaching the Sierra Madre mountains of Mexico ($L_x = 300 \text{ km}$ and $L_y = 1500 \text{ km}$) on a β -plane. The track deflection observed near the large-scale mountain is similar to that found with

group D. With a sufficiently large mountain, the track remains southward, independent of L_y/L_x and R/L_y . Vortex tracks in group E, which features a long mountain ridge, exhibit northward deflection following an earlier upstream southward deflection, when the initial vortex is relatively stronger and larger. This appears to be consistent with the findings of Lin et al. (2005), which indicate that a larger vortex Froude number favors a northward track deflection.

Based on the results in Table 1, southward deflection is typical with a vortex drifting near a relatively larger mountain. Table 2 describes the so-called Taiwan-topography experiments, categorized by groups TN ($L_x = 40 \text{ km}$ and

Table 1. The shallow-water model experiments consist of 80 cases in five groups (A, B, C, D and E) for different basic flow speeds (U), maximum tangential flow speeds (V_{\max}), and the different radii of V_{\max} (R). A Gaussian mountain with a peak height of 4 km is used on an f -plane of 25° N. Maximum upstream track deflection distances in km (positive for northward and negative for southward, defined in the text) for the vortex circulation center (with minimum flow speed) are given in the parentheses. The vortex deflected southward near the mountain may move northward later and the second value in the parentheses denotes the maximum latitudinal distance to the centerline for the vortex center remaining east of the mountain peak. The letter preceding the parentheses indicates the specific case for each group

A: $L_x = 100$ km, $L_y = 200$ km				
$U = -4 \text{ m s}^{-1}$	R (km)			
	100	200	300	400
V_{\max} (m s^{-1})				
10	A (-240,0)	B (-280,0)	C (-320,0)	D (-380,0)
20	E (-280,0)	F (-300,0)	G (-320,0)	H (-320,0)
30	I (-300,0)	J (-240,0)	K (-300,0)	L (-300,0)
40	M (-280,0)	N (-300,0)	O (-300,0)	P (-300,0)
B: $L_x = 100$ km, $L_y = 200$ km				
$U = -8 \text{ m s}^{-1}$	R (km)			
	100	200	300	400
V_{\max} (m s^{-1})				
10	A (-280,0)	B (-280,0)	C (-300,0)	D (-300,0)
20	E (-260,0)	F (-280,0)	G (-300,0)	H (-320,0)
30	I (-240,0)	J (-280,0)	K (-280,0)	L (-280,0)
40	M (-260,0)	N (-260,0)	O (-280,0)	P (-280,0)
C: $L_x = 200$ km, $L_y = 100$ km				
$U = -4 \text{ m s}^{-1}$	R (km)			
	100	200	300	400
V_{\max} (m s^{-1})				
10	A (-240,0)	B (-280,0)	C (-320,0)	D (-340,0)
20	E (-220,0)	F (-240,0)	G (-260,0)	H (-280,0)
30	I (-220,0)	J (-240,0)	K (-240,0)	L (-260,0)
40	M (-220,0)	N (-240,0)	O (-240,0)	P (-220,0)
D: $L_x = 300$ km, $L_y = 600$ km				
$U = -4 \text{ m s}^{-1}$	R (km)			
	100	200	300	400
V_{\max} (m s^{-1})				
10	A (-800,0)	B (-820,0)	C (-840,0)	D (-900,0)
20	E (-780,0)	F (-760,0)	G (-780,0)	H (-800,0)
30	I (-760,0)	J (-740,0)	K (-740,0)	L (-760,0)
40	M (-740,0)	N (-720,0)	O (-720,0)	P (-740,0)
E: $L_x = 400$ km, $L_y = 40$ km				
$U = -4 \text{ m s}^{-1}$	R (km)			
	100	200	300	400
V_{\max} (m s^{-1})				
10	A (-160,0)	B (-200,0)	C (-260,0)	D (-260,0)
20	E (-200,120)	F (-140,240)	G (-160,500)	H (-140,640)
30	I (-140,160)	J (-140,440)	K (-120,900)	L (-120,940)
40	M (-160,160)	N (-120,580)	O (-120,620)	P (-100,600)

Table 2. The shallow-water model experiments for a Gaussian mountain with a peak height of 4 km is used on an f -plane of 25° N. The vortex center and the mountain peak at the departure time are apart with a distance of 800 km. Directions of track deflection (L for leftward and R for rightward) for the vortex circulation center ahead of the terrain centerline for $h = 4$ km are given by the first index in the parentheses, while the second to last index indicate the deflection directions for the slow-moving cases ($U = -2$ and -4 m s $^{-1}$) with $h = 3$ km, 2 km, and 1 km, respectively. Each of the experiment groups (TN and TW) consists of 25 cases that are denoted by A to Y, respectively, for plotting references

TN: $V_{\max} = 40$ m s $^{-1}$, $L_x = 120$ km, $L_y = 40$ km

$R \backslash U$	100	150	200	250	300
-2	A (R, L, L, L)	B (R, L, L, L)	C (R, R, L, L)	D (R, R, L, L)	E (R, R, L, L)
-4	F (R, L, L, L)	G (R, R, L, L)	H (R, R, L, L)	I (R, R, L, L)	J (R, R, L, L)
-6	K (R)	L (R)	M (R)	N (R)	O (R)
-8	P (R)	Q (R)	R (R)	S (R)	T (R)
-10	U (R)	V (R)	W (R)	X (R)	Y (R)

TW: $V_{\max} = 40$ m s $^{-1}$, $L_x = 40$ km, $L_y = 120$ km

$R \backslash U$	100	150	200	250	300
-2	A (L, L, L, L)	B (L, L, L, L)	C (L, L, L, L)	D (L, L, L, L)	E (L, L, L, L)
-4	F (L, L, L, L)	G (L, L, L, L)	H (L, L, L, L)	I (L, L, L, L)	J (L, L, L, L)
-6	K (L)	L (L)	M (L)	N (L)	O (L)
-8	P (L)	Q (L)	R (L)	S (L)	T (L)
-10	U (L)	V (L)	W (L)	X (L)	Y (L)

$L_y = 120$ km) for an equivalently northbound vortex, and TW ($L_x = 120$ km and $L_y = 40$ km) for an equivalently westbound vortex, passing over the idealized CMR. Note that for northbound vortices past the Taiwan mountains, the geometry has been turned 90° so that the basic flow remains easterly. The direction of track deflection is also given for each of the experiments in groups TN and TW. Since some smaller vortices tend to weaken appreciably after traveling a long distance, a shorter departure distance is used in TWA, TWB, TNA, and TNB. Rightward deflection upstream of the mountain is prominent with the vortex tracks of group TN. In the experiment group TW, vortex tracks are deflected primarily leftward. Sensitivity tests with lower mountains were also included for slower basic flow. When the mountain height is decreased in group TN, the rightward deflection may change to leftward deflection. However, the leftward deflection in TW is not changed by varying mountain height. Comparing groups TN and TW (and also several sensitivity tests for circular mountains shown later), in the presence of mean flow, R/L_y appears to be a relevant parameter for determining the direction of track deflection, as also revealed from the scale analysis. Mountain height is also explic-

itly involved in the track deflection for a larger value of R/L_y in TN, which is consistent with the emerging nondimensional parameter in Eq. (10).

5. Discussion of vortex track deflection

5.1 Clockwise- and counterclockwise-curving vortex tracks

In order to understand why the parameter R/L_y plays an important role in affecting vortex track deflection, an experiment (NG) was conducted in a quiescent fluid (i.e., $U = 0$), and with $L_x = 100$ km and $L_y = 200$ km. The vortex center is initialized 200 km east of the mountain peak. Figure 3 shows the vortex circulation and the associated vorticity budgets at 72 h for case NG; the flow pattern at 72 h does not differ appreciably from the flow pattern at 6 h (figures not shown). The evolutions of both vorticity centers and circulation centers are plotted in Fig. 3a and b, respectively. The vortex in case NG moves clockwise around the mountain, in a manner consistent with the findings of Kuo et al. (2001), who conducted a similar experiment using a slightly larger mountain ($L_x = 200$ km and $L_y = 300$ km, the real geographical lengths).

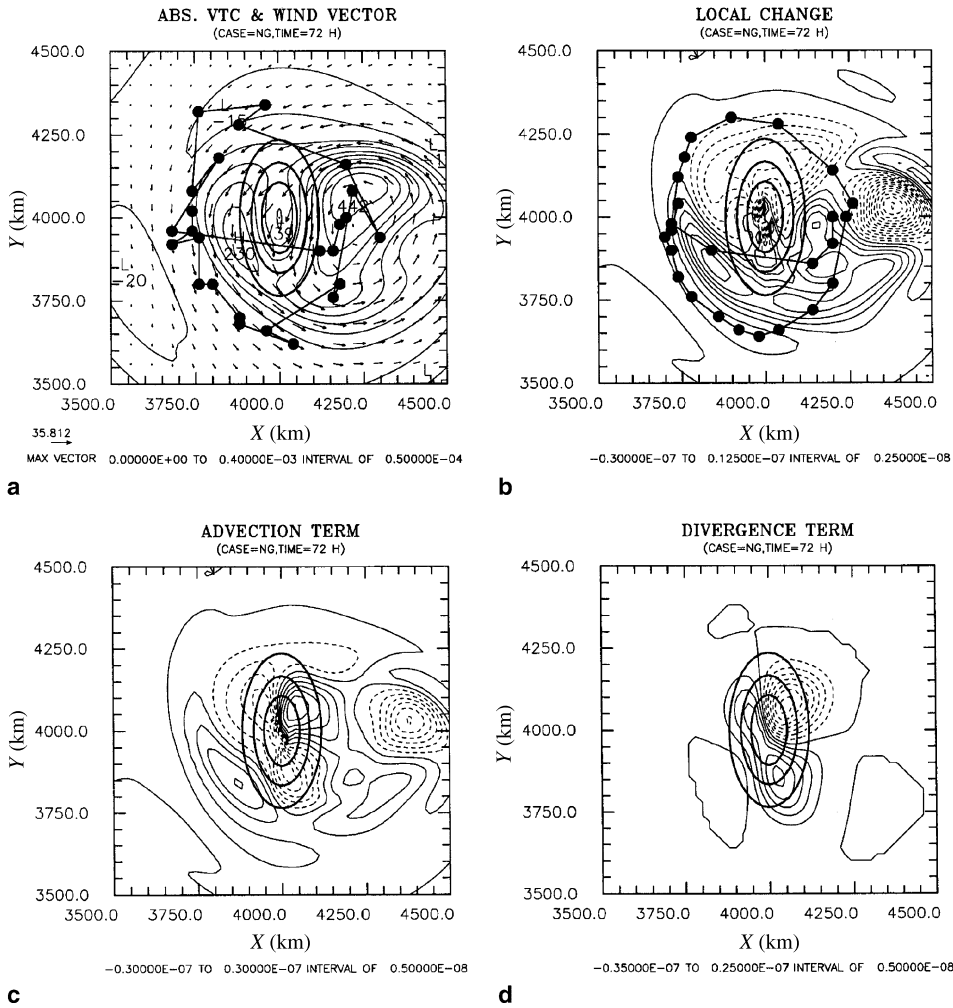


Fig. 3. The simulation results for case NG which is identical to case AN except with the calm basic-wind condition. Shown are the results at 72 h for (a) absolute vorticity (at a contour interval of $0.5 \times 10^{-4} \text{ s}^{-1}$) and wind vector (m s^{-1}), (b) the local time change rate of absolute vorticity (at a contour interval of $2.5 \times 10^{-9} \text{ s}^{-2}$) in the vorticity equation, (c) as in (b) but for the advection term (at a contour interval of $5 \times 10^{-9} \text{ s}^{-2}$), and (d) as in (c) but for the divergence term. Also plotted are solid circles for the vorticity center tracks in (a) and circulation-center tracks in (b) at an interval of 6 h, respectively. The bold lines indicate the contours of 1-km, 2-km and 3-km mountain heights, respectively

The vorticity budgets for case NG indicate that a positive (negative) stretching effect (Fig. 3d) is produced over the downslope (upslope) regions of the mountain. The positive net vorticity budget (Fig. 3b) is present at the southern flank of the vortex, which agrees with the southward motion of the vortex. Apparently, stretching dominates positive (negative) advection to retard (accelerate) vortex motion near the upslope (downslope) regions (Fig. 3c). Thus, it may be concluded that stretching must be present to the southwest of the vortex center for southward deflection to occur.

Based on a series of control experiments for PE vortices, Lin et al. (2005) found that upstream southward (northward) deflection is associated

with stronger (weaker) orographic blocking. They proposed that orographic blocking can be linked to two dominant, nondimensional parameters: the vortex Froude number (V_{max}/Nh), and the effective length scale of the mountain (R/L_y) where L_y herein is the mountain half width in the direction normal to the vortex movement. To further illustrate the significance of these parameters with respect to vortex track deflection in the SW system, a series of experiments (denoted as group C1) were conducted by varying the mountain height used in TWA in a quiescent fluid, and initializing the vortex center at a position 60 km south and 60 km east of the mountain peak. The resulting track (in a period of at least

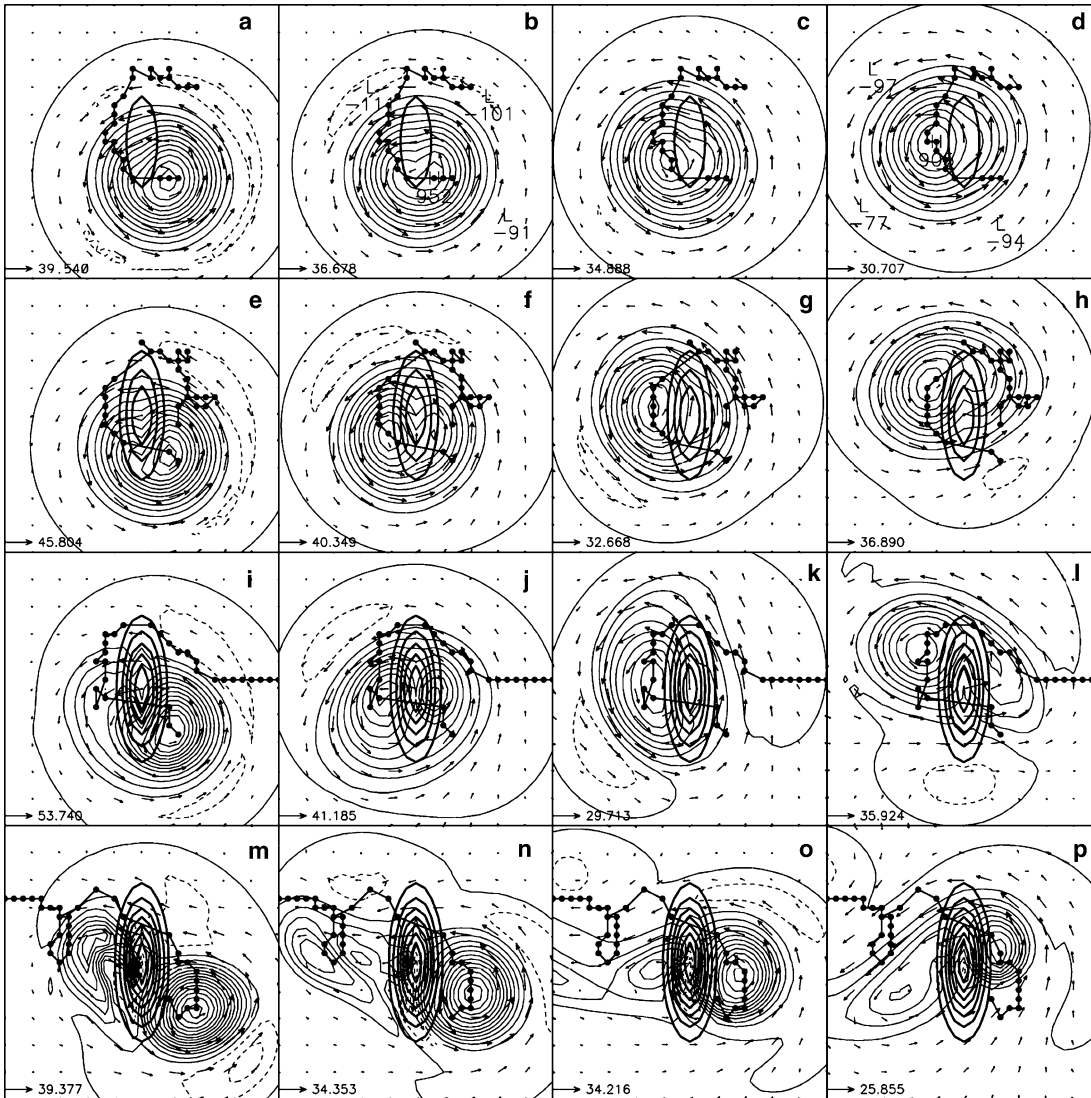


Fig. 4. The simulated absolute vorticity (at a contour interval of 10^{-4} s^{-1}) and flow field for case TWA but in the absence of basic flow for different maximum terrain heights, $h = 1, 2, 3,$ and 4 km (from upper to lower panels). The times presented in the panels from left to right in each row are 6, 12, 18, and 24 h, respectively. The initial vortex center is displayed 80 km southward and 60 km eastward of the mountain peak. Also plotted are solid circles for the vorticity center tracks at an interval of 2 h. The bold lines indicate the contours of mountain heights at an interval of 500 m

48 h) follows a clockwise path when the mountain peak is set below 3 km, but follows a counter-clockwise path when the peak height is increased to 4 km (Fig. 4, the lowest four panels). Additionally, a secondary vortex is generated on the lee side of the 4-km height mountain. Very similar track patterns were found with the experiments C2 (figures not shown), in which the vortex center is initialized at a point 60 km north and 60 km west of the mountain peak. Hence, in both C1 and C2, the vortex is forced into a counter-clockwise track around the higher mountain;

such motion is also observed with experiment group TN.

The vorticity budgets for C1 cases are shown in Fig. 5. Positive vorticity advection is present to the north of the vortex like with case NG, associated with vorticity shrinking in the upslope region, just east of the mountain. Although stretching at the downslope region, just southeast of the mountain, remains strong, the influence of the stretching is essentially counteracted by negative vorticity advection. The net vorticity budget is negative on the southern flank of the vortex,

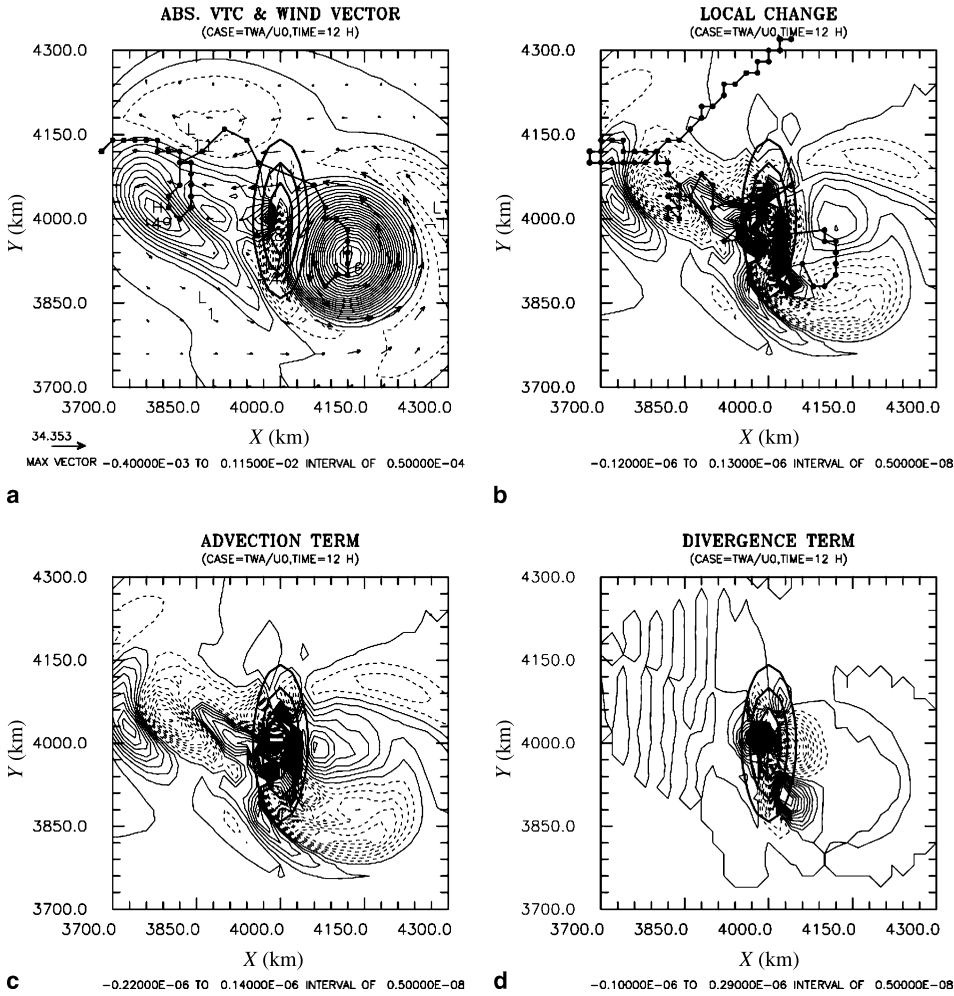


Fig. 5. The simulation results at 12 h for case TWA but in the absence of basic flow. (a) Absolute vorticity (at a contour interval of $0.5 \times 10^{-4} \text{ s}^{-1}$) and the flow field, (b) the net time change rate of absolute vorticity (at a contour interval of $0.5 \times 10^{-8} \text{ s}^{-2}$) in the vorticity equation, (c) as in (b) but for the advection term and (d) as in (b) but for the divergence term. Also plotted are solid circles for the vorticity-center tracks in (a) and the circulation center track in (b) at an interval of 2 h. The bold lines indicate the contours of 1-km, 2-km and 3-km mountain heights, respectively

and is positive to the east of the mountain and along the northern flank of the vortex; consequently, the vortex is deflected northward. When the mountain height is lowered to 2 km, the advection and stretching nearly counteract each other, but vortex stretching is overwhelmingly large along the western and southern slopes of the mountain (not shown). The vortex center appears to jump over the southern portion of this lower mountain and move in a clockwise sense. The downstream advance of the stretching forces the vortex to move in clockwise pattern. Thus, the effect of vortex stretching (divergence) is more favorable for leftward deflection of a vortex past an isolated mountain as found for an upslope and leftward barotropic vortex when placed over the topographic slope of a long ridge (Grimshaw et al. 1994).

Uniform flow traversing a mountain range is well known to deflect leftward due to the imbalance of the pressure gradient force and the re-

duced Coriolis force in the vicinity of the mountain (e.g., fig. 4a in Lin et al. 1999). From case TWB (Fig. 6a), the quasi-steady flow at 46 h exhibits leftward deflection upstream of the mountain. The initial vortex (inserted at 48 h) essentially follows the basic flow, even as the parent vortex has passed downstream of the mountain (Fig. 6b). At 70 h, the vortex has been deflected southward upstream, where the flow becomes more northerly in the western flank of the shrinking vortex. This northerly component of the asymmetric flow exists just upstream and northeast of the mountain (figures not shown) and is likely responsible for the southward deflection of the vortex. This is consistent with the argument proposed in Lin et al. (1999).

5.2 Control parameters

We have discussed the mechanisms for both the northward and southward deflections of a vortex

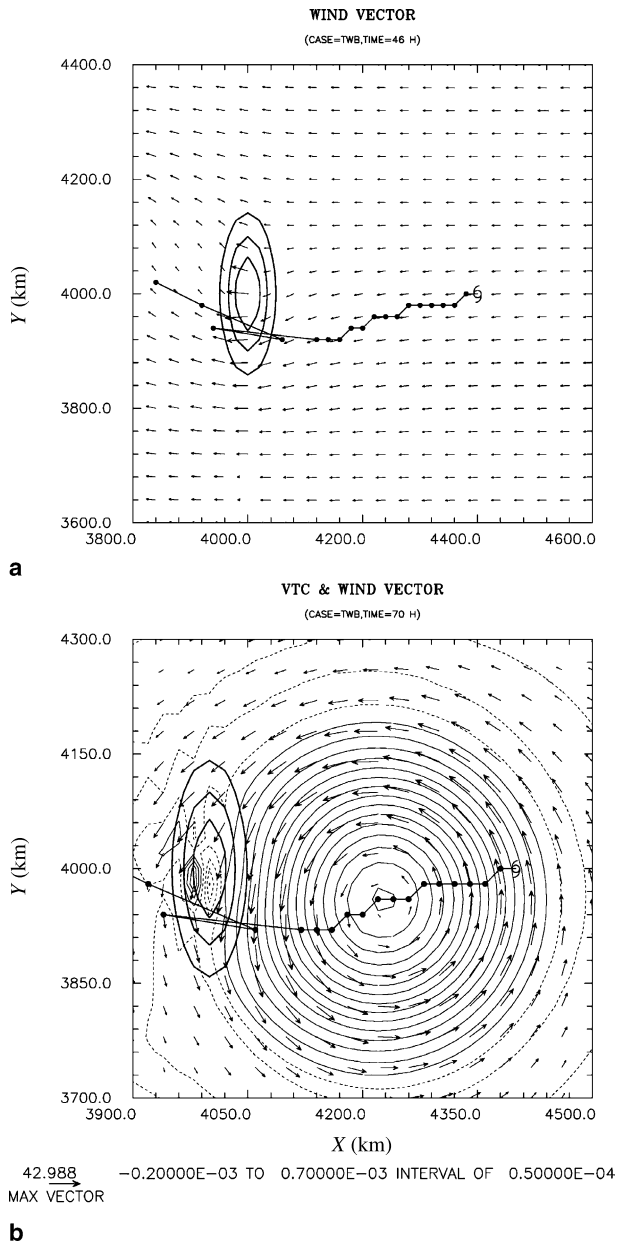


Fig. 6. The flow field for case TWB (a) at 46 h which is 2 h prior to the release time of the vortex, and (b) at 70 h. The initial vortex is denoted by the typhoon symbol at a departure distance of 400 km upstream of the mountain peak. Also plotted are solid circles for circulation center tracks an interval of 2 h. The bold lines indicate the contours of 1-km, 2-km and 3-km mountain heights, respectively

encountering mesoscale mountains and steered by the basic flow. In the absence of the basic flow, all of the vortices in the experiments of groups A through D in Table 1 are trapped and move clockwise around the mountain, as found with case NG. In order for a vortex to become trapped, the length scale of the mountain must be greater than the

radius of maximum tangential flow speed, R . A larger mountain may more easily trap a vortex, except when the basic flow is sufficiently strong. We have found that none of the vortices, with varying values of R and V_{\max} , will be trapped by the mountain if the basic flow is increased, for example, to 8 m s^{-1} . It may be concluded that the steering flow does not play a role in changing the direction of vortex deflection, despite the fact that it has contributions to leftward deflection. This implies that the basic-flow Froude number is not a dominant parameter in determining rightward or leftward track deflection, as compared to other more dominant parameters. As was shown by Kuo et al. (2001), we found that the clockwise motion of a vortex around a mountain is reduced with increasing vortex size. There is no clockwise motion with a vortex defined with $R > 200 \text{ km}$ ($\sim 2 L_y$) on an f -plane environment. The patterns of the SW vortex tracks in an f -plane environment are consistent with the PE vortex tracks around a mesoscale mountain from Lin et al. (2005).

For a SW vortex, we need to link the mechanisms of northward and southward deflections in terms of relevant physical parameters. Similar to Smith et al. (1997) and Kuo et al. (2001) summarized some common patterns in the circulating paths of β -drifting vortices in terms of two non-dimensional parameters, L_m/R and β/β_e , where β_e is the so-called orographic β -effect, defined as $\beta_e = fh/HL_m$. In the SW system, the flow regimes for wake vortices, resulting from uniform flow past a mountain obstacle, can be identified with respect to nondimensional mountain height and basic-flow Froude number (Schär and Smith 1993a, b; Nadiga et al. 1996). We may also expect that vortex track deflection can be better explained through the examination of two non-dimensional parameters. Based on the sensitivity tests (discussed later), we may drop f and g in the formulations so that the gravity wave speed and the Rossby radius of deformation will not be relevant to the direction of track deflection; however, they will affect the magnitude of the deflection. Thus, the formulations of the nondimensional parameters for vortex track deflection on an f -plane may be somewhat different from those for a β -drifting vortex (Zehnder and Reeder 1997).

Figure 7a depicts the regimes of the vortex track deflection with respect to the nondimensional parameters (HL_m/hR) and (V_{\max}/U) from

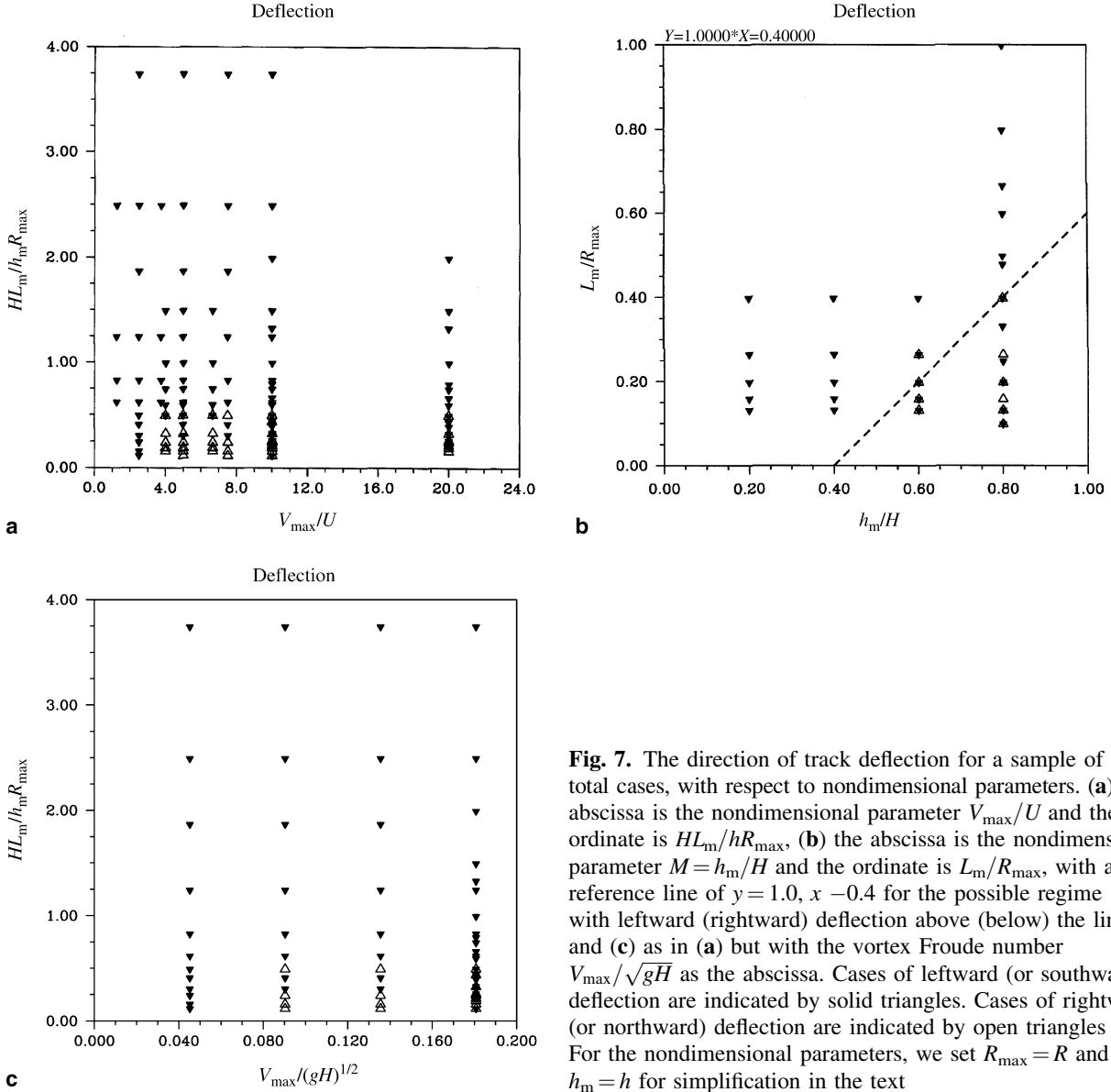


Fig. 7. The direction of track deflection for a sample of 200 total cases, with respect to nondimensional parameters. **(a)** The abscissa is the nondimensional parameter V_{\max}/U and the ordinate is HL_m/hR_{\max} , **(b)** the abscissa is the nondimensional parameter $M = h_m/H$ and the ordinate is L_m/R_{\max} , with a reference line of $y = 1.0, x = 0.4$ for the possible regime with leftward (rightward) deflection above (below) the line and **(c)** as in **(a)** but with the vortex Froude number V_{\max}/\sqrt{gH} as the abscissa. Cases of leftward (or southward) deflection are indicated by solid triangles. Cases of rightward (or northward) deflection are indicated by open triangles (Δ). For the nondimensional parameters, we set $R_{\max} = R$ and $h_m = h$ for simplification in the text

the above experiments (more than 200 cases). Herein, in the presence of mean flow, L_m is represented by L_y . The presence of U here may account for the effect of the slightly southward deflection of the environmental flow (due to orographic effects) and also formulates a nondimensional form in the abscissa. The parameter, V_{\max}/U , is also the ratio of the vortex Froude number and basic-flow Froude number, which represents the competition between the vortex and basic flow when interacting with the topography. As seen in the figure, leftward deflection occurs for very small values of V_{\max}/U regardless of the value of HL_m/hR . Most instances of rightward deflection occur with moderate values

of V_{\max}/U and very small values of HL_m/hR . For $V_{\max}/U > 10$, either rightward or leftward deflection is possible if $HL_m/hR < 0.5$, above which only leftward deflection occurs. Small values of HL_m/hR also correspond to large R/L_m , for which rightward deflection is more likely to occur with a northbound vortex, as shown in the TN experiments. If the parameter of V_{\max} can be dropped in determining the direction of track deflection, then the nondimensional parameter HL_m/hR can be decomposed into two other nondimensional parameters: the inverse nondimensional vortex size, L_m/R , and the nondimensional mountain height, h/H (Fig. 7b). Note that in Fig. 7b only a sub-domain of Fig. 7a is plotted

for clarity. Leftward deflection of a vortex is more likely to occur for larger values of L_m/R and smaller values of h/H . Again, either leftward or rightward track deflection can occur for small values of L_m/R and large values of h/H . Rightward deflection will be possible only for $h/H \geq 0.4$ for a blade-shaped mountain. Consistently, most cases of leftward deflection occur with $L_m/R \geq 0.3$, based on analysis of the above nondimensional parameter regimes. For a vortex of $R = 300$ km, leftward deflection tends to occur if $L_m > 90$ km; this tendency is reflected from the TW experiments, with $L_m = 120$ km and $R \leq 300$ km. In summary, a vortex is deflected leftward for larger L_m/R and smaller h/H ; otherwise, either leftward or rightward deflection is possible.

The results presented in Tables 1 and 2 indicate that the intensity of basic flow does affect the vortex track deflection, as was previously discussed. The magnitude of track deflection, whether leftward or rightward, decreases as the basic flow speed increases, as has been revealed through observations (Yeh and Elsberry 1993a) and through modeling experiments (Lin et al. 2005). On the other hand, the direction of deflection varies with vortex Froude number, as shown in a plot of HL_m/hR versus the vortex Froude number (Fig. 7c). As a consequence, leftward deflection of a vortex is more likely to occur with a smaller vortex Froude number. Based on control experiments for a PE vortex encountering a mesoscale mountain, Lin et al. (2005) concluded

that rightward (northward) deflection increases for larger vortex Froude numbers when R/L_m is not small. From our SW experiments, the deflection is always southward when R/L_m is small, regardless of the vortex intensity and, consequently, the vortex Froude number.

With the idealized CMR, either rightward or leftward deflection can occur for different sets of the parameters. In previous experiments involving the terrain of Taiwan, we have varied the mountain height, the basic flow intensity, and the vortex size. For a northbound (westbound) vortex, the rightward (leftward) track deflection is more likely to occur, indicating that the parameters R/L_m and h/H significantly affect vortex track deflection. However, Fig. 7a indicates that the direction of deflection will be changed from southward for smaller values of V_{\max} to northward for larger values of V_{\max} , along $HL_m/hR = 0.25$. In both the TW and TN experiments, we have used a fixed value of $V_{\max} = 40$ m s⁻¹. Therefore, we will revisit this transition in the direction of track deflection for a relatively weaker and larger vortex ($V_{\max} = 30$ m s⁻¹ and $R = 200$ km) and a high mountain ($h = 4$ km) with respect to different mountain lengths, L_x and L_y .

Figure 8 shows the maximum deflection distances for a westward moving vortex past a mountain with various combinations of L_x and L_y . Herein, L_y in this case is also equivalent to the mountain half width in the direction normal to the vortex movement. It is interesting to see

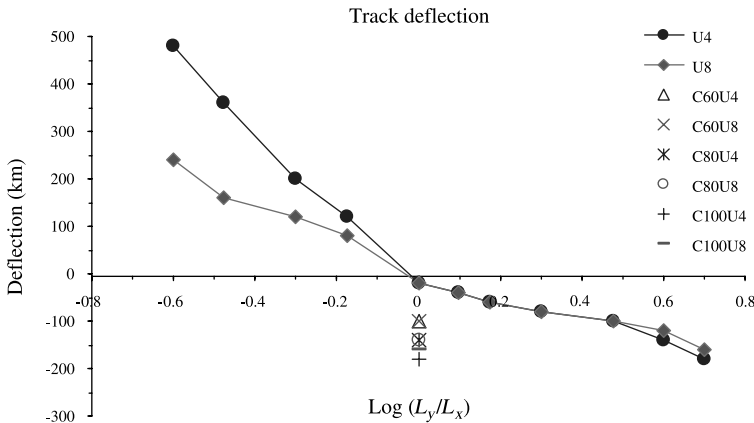


Fig. 8. Plots of the maximum track deflection distance (km) for a vortex with R (200 km) and V_{\max} (30 m s⁻¹) fixed with respect to varying L_y and L_x , both starting from 40 km, over a hill of 4 km height in a fluid depth of 5 km. The results are for different steering flow speeds of $U = -4$ m s⁻¹ (circles) or -8 m s⁻¹ (diamonds). Positive ordinate values are for northward deflection and negative for southward. The leftmost points represent $L_y = 40$ km and $L_x = 160$ km and the rightmost points $L_y = 200$ km and $L_x = 40$ km. Case $CaUb$ is for the vortex at $U = -b$ m s⁻¹ past a circular mountain with $L_x = L_y = a$ km

that northward (southward) deflection occurs when the circular mountain ($L_x = L_y = 40$ km) is changed to a more (less) elliptical mountain, with the major axis in the direction of the vortex motion. Generally, a more eccentric elliptical

mountain leads to an increase in the maximum deflection distance. The maximum distance of southward deflection is nearly equal to the value of L_y (the longer axis in this case) while the maximum distance of northward deflection is nearly

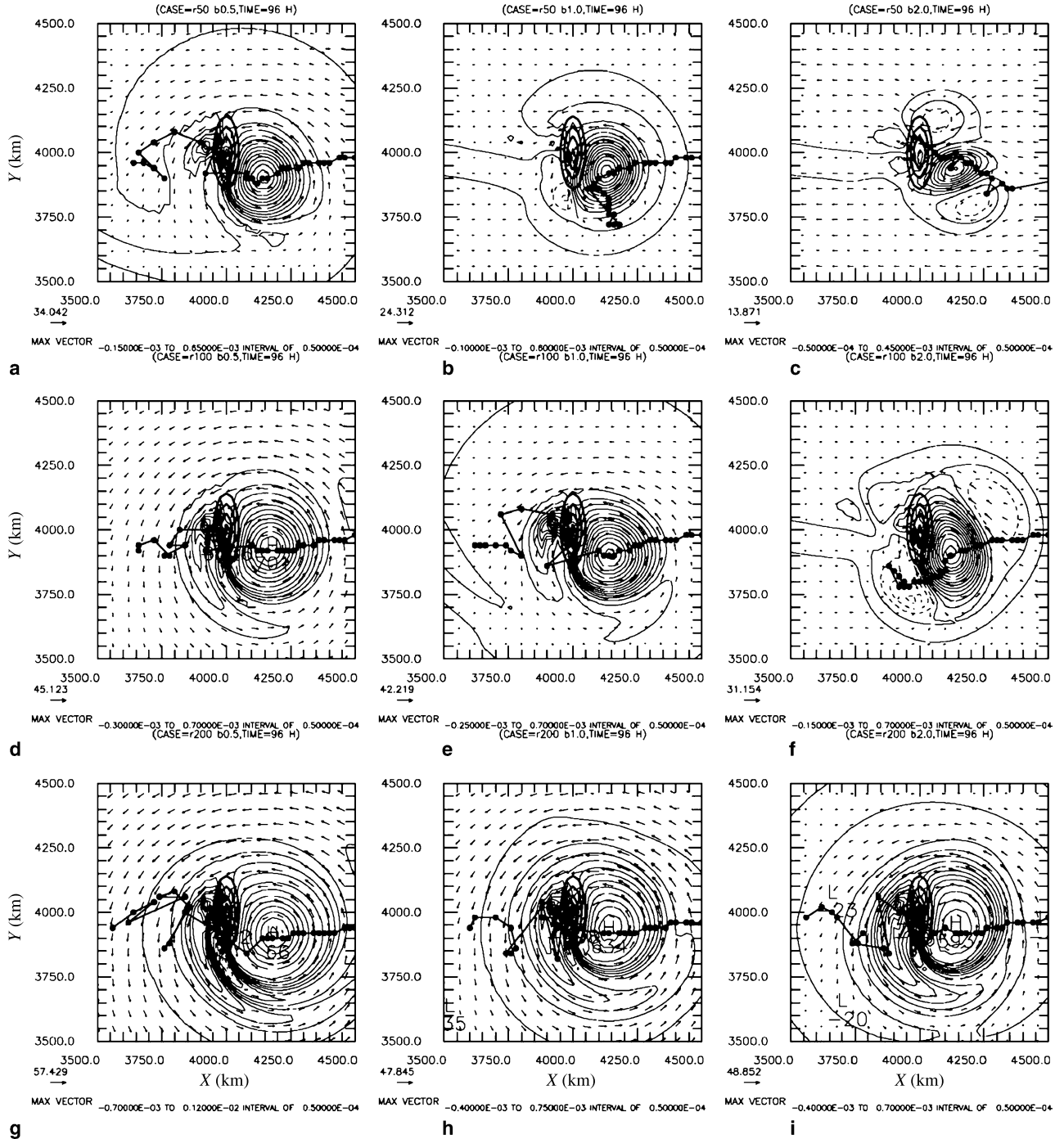


Fig. 9. The absolute vorticity (at a contour interval of $0.5 \times 10^{-4} \text{ s}^{-1}$) and flow field at 98 h for cases TW ($V_{\max} = 40 \text{ m s}^{-1}$ and $U = -4 \text{ m s}^{-1}$) with different sets of $(R, b) =$: (a) (50 km, 0.5), (b) (50 km, 1), (c) (50 km, 2), (d) (100 km, 0.5), (e) (100 km, 1), (f) (100 km, 2), (g) (200 km, 0.5), (h) (200 km, 1), and (i) (200 km, 2). Also plotted are the solid circles denoting circulation-center tracks at intervals of 2 h. Maximum wind speed is indicated at the lower left corner in each panel. The bold lines indicate the contours of 1-km, 2-km and 3-km mountain heights, respectively

three times the value of L_x (the longer axis in this case). Doubling the basic flow speed leads to a slight reduction of southward deflection, but a greater reduction of northward deflection. For all circular mountains of $L_x > 60$ km, the vortex is always deflected southward, and this deflection increases with increased L_x . Sensitivity to the eccentricity of the elliptical topography may explain why rightward deflection is more likely to occur with northbound typhoons encountering the CMR.

5.3 Sensitivity tests on the vortex profile, reduced gravity, and the Coriolis parameter

To avoid confusion, and to clarify more important parameters for controlling deflection's direction, we dropped several physical factors from the previous synthesis: the vortex profile (b), reduced gravity (g) and the Coriolis parameter (f). A vortex track affected by β -drift may be sensitive to the parameter b in Eq. (1) used for the

determination of a radial vortex profile (e.g., Fiorino and Elsberry 1989; Smith 1993). A larger value of b will give a narrower vortex core with stronger radial gradients of tangential flow speed (cf. fig. 1 of Smith et al. 1997). Since the initial vortex is a function of both b and R , these two parameters actually control the structure of the vortex circulation. Figure 9 shows the results of sensitivity tests using different sets of b and R for a vortex with $V_{\max} = 40 \text{ m s}^{-1}$ and $U = -4 \text{ m s}^{-1}$. For a fixed value of R , track deflection is independent of the parameter b except with the tiny vortex defined by $b = 2$ and $R = 50 \text{ km}$ (Fig. 9c). This small, weakened vortex is deflected southward by the topography earlier, then is redirected northward. A vortex with $b = 0.5$ and $R = 200 \text{ km}$ appears to be too large when compared with the size of the topography (Fig. 9g). Vortices defined by $b = 2$ with $R = 50 \text{ km}$, and by $b = 0.5$ with $R = 200 \text{ km}$, are two extreme cases in our study, yet a change in the direction of track deflection is

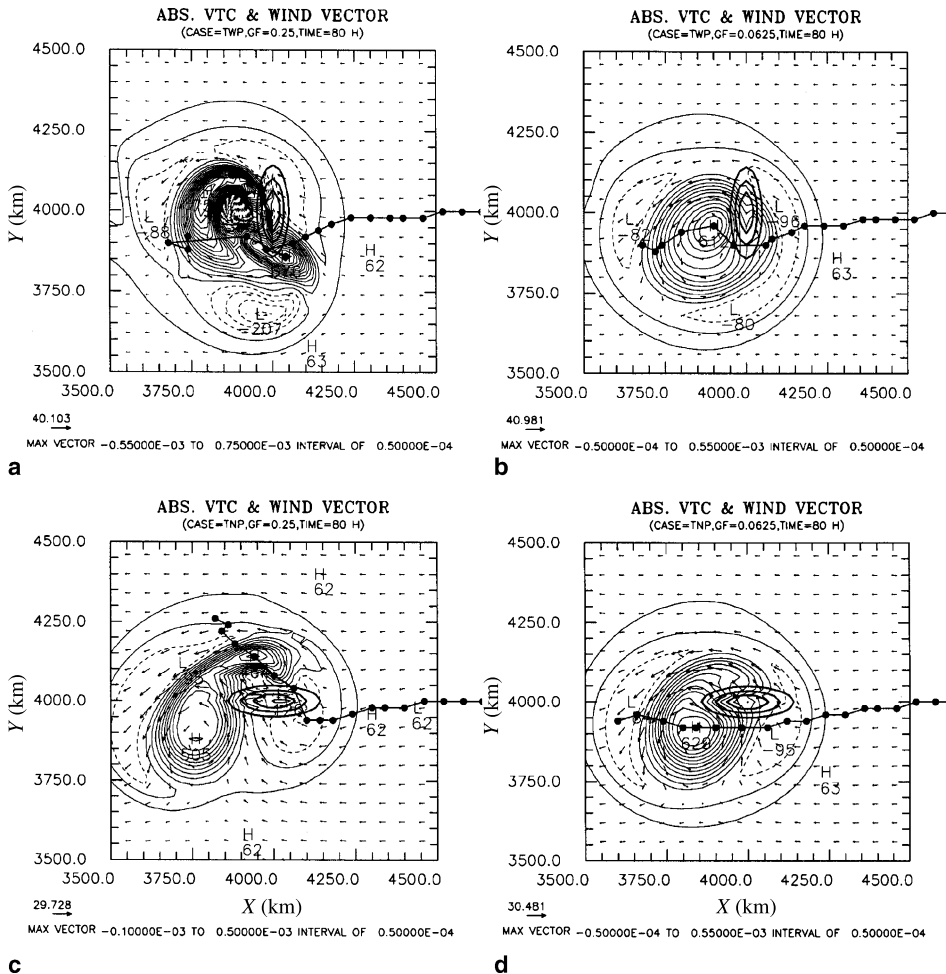


Fig. 10. The absolute vorticity (at a contour interval of $0.5 \times 10^{-4} \text{ s}^{-1}$) and flow field for the sensitivity tests on the reduced gravity (a) by a factor of 1/4 as for case TWP at 80 h, (b) as in (a) but by a factor of 1/16, and (c) as in (a) but for case TNP and (d) as in (b) but for case TNP. The initial vortex is displayed at a departure distance of 800 km upstream of the mountain peak. Also plotted are solid circles for vorticity-center tracks an interval of 2 h. The bold lines indicate the contours of 1-km, 2-km and 3-km mountain heights, respectively

not directly caused by the parameter b in these experiments. Other previous numerical studies from Smith et al. (1997) indicate that the β -drift speed of the SW vortex is proportional to $1/b$ and R , while the direction of vortex motion is nearly invariant for different values of b . For track deflection in an f -plane environment, other parameters appear to be more dominant than the parameter b .

In both the TN and TW experiments, the direction of track deflection is not sensitive to the Coriolis parameter f . With f set for 25° N and for 45° N, the propagation speeds of the lee vortex (northwest of the mountain) in these simulations are faster than for $f=0$. Upstream movement of the primary vortex is not sensitive to f . The Coriolis parameter may be more relevant in the evolution of the vortex later in the simulation, but is less influential to the direction of vortex track deflection upstream of the mountain. The result is consistent with the SW vortex track of Kuo et al. (2001), in which an increase of planetary vorticity results in a faster looping of the vortex on an f -plane, as well as on a β -plane, but never results in a change in the direction of the movement. The result indicates that the Rossby number is not a parameter controlling the direction of track deflection for the SW vortex, which is consistent with the PE model results in Lin et al. (2005).

Reduced gravity in the SW system can be analogous to weaker stratification in a stratified flow system. As shown by Zehnder and Reeder (1997), the southward deflection for a vortex near a large-scale, elliptical mountain is significantly increased as the reduced gravity in the control run (3.43 m s^{-2}) is decreased by a factor of 6 to 0.58 m s^{-2} . Figure 10 shows the results at 80 h for our cases TWP and TNP, with the gravity reduced by a factor of 4 and 16. The vortex tracks are not altered significantly by the varied gravity. However, the vortex track is somewhat sensitive to the significantly reduced gravity in the TNP simulation (Fig. 10d) in which the reduction of gravity by a factor of 16 has resulted in a change in direction of track deflection, from northward in TNP with the normal gravity to southward in the reduced gravity case. The vortex advances closer to the mountain while deflected southward early in the simulation, but then the primary vortex is trapped to the south of the mountain. For varying gravity, the track and structure of the

upstream vortex remains similar in both TWP and TNP. The sensitivities of a vortex track to the largely reduced gravity, near mesoscale mountains as shown here, are consistent with those near a large-scale mountain found by Zehnder and Reeder (1997).

6. Concluding remarks

This study utilizes a SW numerical model to explore the influences of mesoscale mountains on an approaching vortex. In order to simplify the dynamics, we focus on the vortex encountering mesoscale mountains in an f -plane environment. For the orographically induced β -drift, systematic experiments indicate that a moving vortex can be deflected rightward or leftward on the upstream side of the mountain, and that the direction of deflection is dependent on several parameters: the initial maximum tangential speed of the vortex (V_{\max}), the basic flow intensity (U), the fluid depth (H), the radius of V_{\max} (R), and the relevant mountain half-width (L_m). Here, in the presence of mean flow, L_m is represented by L_y defined as the mountain half width in the direction normal to the vortex movement. The sensitivity experiments also indicate that different vortex profiles, reduced gravity, and the Coriolis parameter do not significantly affect the direction of vortex track deflection; instead, the direction of track deflection is sensitive to the effective ratio of R/L_m and the mountain height h . The nondimensional parameters, the vortex Froude number, V_{\max}/\sqrt{gH} , the basic-flow Froude number, U/\sqrt{gH} , and the vortex aspect ratio, R/L_m , thus are to be considered in determining the direction of track deflection.

Examination of parameter regimes shows that when R/L_m is not small, the vortex Froude number becomes more important than the basic-flow Froude number in determining the direction of vortex track deflection. The direction of track deflection is largely controlled by the nondimensional vortex size (R/L_m) with respect to the nondimensional height (h/H). If the nondimensional parameter (HL_m/hR) is larger than 0.5, the southward (or leftward facing downstream) deflection seems to be satisfied for the vortex. Southward deflection could be attributed more to a smaller vortex Froude number. However, a large vortex Froude number does not necessarily support

northward track deflection when $HL_m/hR < 0.5$, where both northward and southward deflection are possible. For more typical conditions with $h/H < 0.8$, northward (or rightward) deflection will not appear with more strictly, $R/L_m < 3.33$. For $R/L_m < 2.50$, a vortex is always deflected southward (leftward), regardless of the mountain height, the vortex intensity, and the vortex Froude number, which agrees with Zehnder and Reeder (1997) and Kuo et al. (2001).

Without explicit horizontal momentum diffusion, the vorticity budgets are essentially determined by vorticity advection and vorticity stretching (or divergence effect) in the vertical vorticity equation, with the former (latter) being more likely responsible for the northward (southward) deflection of a westbound vortex. Without the steering of basic flow, a vortex initialized near the mountain will tend to follow a clockwise track around a wider and lower mountain. When the mountain is sufficiently high, the vortex track becomes counter-clockwise, due to more dominant vortex advection. We also found that there is a transition from leftward to rightward track deflection for a vortex impinging upon a mountain of decreasing L_m . This indicates that rightward (leftward) track deflection will be predominant for a northbound (westbound) vortex encountering mesoscale topography similar to the CMR. Such a variation in the direction of track deflection, with respect to height and aspect ratio (L_y and L_x) of mesoscale mountains, has not been explicitly addressed in the literature. It was shown in this study that the amount of deflection is intimately related to both L_x and L_y . More experiments will be needed to identify complicated relations for the degree of track deflection, and such a study will be conducted later.

In Lin et al. (2005), leftward (rightward) deflection is more likely to occur with a westbound PE vortex of a smaller (larger) vortex Froude number when R/L_y is not large. In their study, the relation of track deflection to the parameter R/L_y is not explicitly established. We have constructed non-dimensional parameter regimes for determining vortex track deflection by combining the parameter R/L_y with the nondimensional mountain height (h/H), and the results are consistent with previous PE modeling studies (Huang and Lin 1997; Lin et al. 1999, 2002, 2005). Leftward or rightward deflection exists in the parameter re-

gime, but a regime of leftward deflection is clearly defined in terms of the examined parameters at their normal scales. Our SW modeling results promote specific parameters controlling deflection in the track of a vortex upstream of mesoscale mountains. A PE model will be utilized to investigate deflection in the tracks of more realistic typhoons, near mesoscale mountains and within a stratified fluid, in a companion study.

Appendix

The 2D SW equations for homogeneous fluid are given by

$$\frac{\partial u}{\partial t} = -u \frac{\partial u}{\partial x} - v \frac{\partial u}{\partial y} - g \frac{\partial h'}{\partial x} + fv, \quad (\text{A.1})$$

$$\frac{\partial v}{\partial t} = -u \frac{\partial v}{\partial x} - v \frac{\partial v}{\partial y} - g \frac{\partial h'}{\partial y} - fu, \quad (\text{A.2})$$

$$\frac{\partial h'}{\partial t} = -\frac{\partial u(h' - h_B)}{\partial x} - \frac{\partial v(h' - h_B)}{\partial y} - H_0 \left(\frac{\partial u}{\partial x} + \frac{\partial v}{\partial y} \right), \quad (\text{A.3})$$

or an equivalent advection form,

$$\begin{aligned} \frac{\partial h'}{\partial t} = & -u \frac{\partial h'}{\partial x} - v \frac{\partial h'}{\partial y} + u \frac{\partial h_B}{\partial x} + v \frac{\partial h_B}{\partial y} \\ & - (h' + H_0 - h_B) \left(\frac{\partial u}{\partial x} + \frac{\partial v}{\partial y} \right), \end{aligned} \quad (\text{A.4})$$

where $h' = h - H_0$, the deviation of the upper surface height h of the fluid from its initial unperturbed constant height H_0 , and h_B the height of the bottom topography. The mountain is described by a Gaussian function as

$$h_B = h \exp \left[-\left(\frac{x - x_c}{L_x} \right)^2 - \left(\frac{y - y_c}{L_y} \right)^2 \right], \quad (\text{A.5})$$

where x_c and y_c are the coordinates of the peak, and L_x and L_y are the approximate half-width values of the mountain in the x - and y -direction, respectively. The initial surface height perturbation consists of two parts, resulting from geostrophic balance of the basic flow and gradient balance of the vortex. The vortex part is solved from the nondivergent balance equation, which can be obtained by computing divergence of the momentum equations (A.1) and (A.2). A horizontal mixing term is added into (A.4) to account for turbulent mixing for flow passage over steeper slopes, taking the form of

$$\frac{\partial}{\partial x} \left(K_H \frac{\partial h'}{\partial x} \right) + \frac{\partial}{\partial y} \left(K_H \frac{\partial h'}{\partial y} \right)$$

where $K_H = c_H \Delta x \Delta y [(u_x^2 + v_y^2) + 0.5(v_x + u_y)^2]^{1/2}$ with constant c_H for a nonlinear diffusion term. A value of 2 is adopted for c_H in this study. We found that moderate diffusion is required to modulate developing lee waves when the stronger flow of the vortex core is impinging on a steep mountain, as found in Nadiga et al. (1996). Inclusion of the horizontal diffusion also provides a mimic process in nature. The introduction of the horizontal mixing in the surface height pertur-

bation equation does not produce any vertical vorticity, as the curl of the pressure gradient force is zero.

In order to remove the nonlinear aliasing errors associated with waves of two grid intervals, a linear filter consisting of smoother and desmoother (Shapiro 1975) has been applied to the prognostic variables after each time step integration. The advection scheme adopts a semi-Lagrangian treatment which computes the advected quantity at the estimated departure point by Lagrange interpolation. The computation is first conducted for the advection in the x -direction and then for the y -direction with the updated former advection effect, as a split manner to allow faster calculation. In the model, we have adopted a split advection scheme with cubic Lagrange interpolation. A unsplit scheme can also be applied to compute the advection simultaneously for both x - and y -directions, e.g., using bi-cubic or bi-quintic Lagrange interpolation. The time-differencing is forward in time, which is conditionally stable if the updated momentum is used to predict height perturbations (see Pielke 1984). More advanced schemes combining the explicit time and semi-implicit time schemes can be developed to increase the accuracy and also maintain better stability for SW models (e.g., Dubois et al. 2005).

Acknowledgments

Discussions with Dr. H.-C. Kuo, Dr. C.-C. Wu, and Mr. S.-T. Wang were helpful for this study. The proofreading of the manuscript by Chris Hill is appreciated. This study is supported by National Science Council of Taiwan under projects Grant NSC 93-2119-M-008-008-AP1 and NSC 94-2111-M-008-113-AP1.

References

Bender MA, Tuleya RE, Kurihara Y (1987) A numerical study of the effect of island terrain on tropical cyclones. *Mon Wea Rev* 115: 130–55

Chan JC-L, Williams RT (1987) Analytical and numerical studies of the beta-effect in tropical cyclone motion: Part I. Zero mean flow. *J Atmos Sci* 44: 1257–65

Chang SW (1982) The orographic effects induced by an island mountain range on propagating tropical cyclones. *Mon Wea Rev* 110: 1255–70

DeMaria M (1985) Tropical cyclone motion in a nondivergent barotropic model. *Mon Wea Rev* 113: 1199–210

Dubois T, Jauberteau F, Temam RM, Tribbia J (2005) Multilevel schemes for the shallow water equations. *J Compu Phys* 207: 660–94

Fiorino M, Elsberry RL (1989) Some aspects of vortex structure related to tropical cyclone motion. *J Atmos Sci* 46: 975–90

Grimshaw R, Tang Y, Broutman D (1994) The effect of vortex stretching on the evolution of barotropic eddies over a topographic slope. *Geophys Astrophys Fluid Dynamics* 76: 43–71

Huang C-Y, Lin Y-L (1997) The evolution of mesoscale vortex impinging on symmetric topography. *Proc Natl Sci Counc* 21: 285–309

Kuo H-C, Williams RT, Chen J-H, Chen Y-L (2001) Topographic effects on barotropic vortex motion: no mean flow. *J Atmos Sci* 58: 1310–27

Lin Y-L (2007) *Mesoscale dynamics*. Cambridge University Press (to appear)

Lin Y-L, Han J, Hamilton DW, Huang C-Y (1999) Orographic influence on a propagating cyclone. *J Atmos Sci* 56: 534–62

Lin Y-L, Ensley DB, Chiao S, Huang C-Y (2002) Orographic influences on rainfall and track deflection associated with the passage of a tropical cyclone. *Mon Wea Rev* 130: 2929–50

Lin Y-L, Chen S-Y, Hill CM, Huang C-Y (2005) Control parameters for the influence of a mesoscale mountain range on cyclone track continuity and deflection. *J Atmos Sci* 62: 1849–66

Nadiga BT, Margolin LG, Smolarkiewicz PK (1996) Different approximations of shallow fluid flow over an obstacle. *Phys Fluid* 8: 2066–77

Pielke RA (1984) *Mesoscale meteorological modeling*. Academic Press, New York, 632 pp

Schär C, Smith RB (1993a) Shallow-water flow past isolated topography: Part I. Vorticity production and wake formation. *J Atmos Sci* 50: 1373–400

Schär C, Smith RB (1993b) Shallow-water flow past isolated topography: Part II. Transition to vortex shedding. *J Atmos Sci* 50: 1401–12

Shapiro R (1975) Linear filtering. *Math Comp* 29: 1094–7

Shapiro LJ, Ooyama KV (1991) Barotropic vortex evolution on a beta plane. *J Atmos Sci* 47: 170–87

Smith RB (1993) A hurricane beta-drift law. *J Atmos Sci* 50: 3213–5

Smith RB, Smith DF (1995) Pseudoinviscid wake formation by mountains in shallow-water flow with a drifting vortex. *J Atmos Sci* 52: 436–54

Smith RB, Li X, Wang B (1997) Scaling laws for barotropic vortex beta-drift. *Tellus* 49A: 474–85

Smolarkiewicz PK, Rotunno R (1989) Low Froude number flow past three dimensional obstacles: Part I. Baroclinically generated lee vortices. *J Atmos Sci* 46: 1154–64

Wang ST (1980) Prediction of the behavior and strength of typhoons in Taiwan and its vicinity. Research Report 108, Chinese National Science Council, Taipei, Taiwan, 100 pp (in Chinese)

Wedi NP, Smolarkiewicz PK (2003) Extending Gal-Chen and Somerville terrain-following coordinate transformation on time-dependent curvilinear boundaries. *J Compu Phys* 193: 1–20

Yeh T-C, Elsberry RL (1993a) Interaction of typhoons with the Taiwan orography: Part I. Upstream track deflections. *Mon Wea Rev* 121: 3193–212

Yeh T-C, Elsberry RL (1993b) Interaction of typhoons with the Taiwan orography: Part II. Continuous and discontinuous tracks across the island. *Mon Wea Rev* 121: 3213–33

Zehnder JA (1993) The influence of large-scale topography on barotropic vortex motion. *J Atmos Sci* 50: 2519–32

Zehnder JA, Reeder MJ (1997) A numerical study of barotropic vortex motion near a large-scale mountain range with application the Sierra Madre. *Meteorol Atmos Phys* 64: 1–19